Crustal Deformation Pattern on the Northeastern Margin of the Tibetan Plateau derived from GPS Observations

Sihan Yu and Xiaoning Su *

Posted Date: 17 April 2023

doi: 10.20944/preprints202304.0378.v1

Keywords: Crustal deformation; Haiyuan-Liupanshan fault zone; Slip rate; Locking depth; Slip deficit rate

Article

Crustal Deformation Pattern on the Northeastern Margin of the Tibetan Plateau Derived from GPS Observations

Sihan Yu and Xiaoning Su *

Lanzhou Jiaotong University,Lanzhou 730000,China; 12201867@stu.lzjtu.edu.cn (S.Y.)
* Correspondence: Xiaoning Su (suxiaoning_666@mail.lzjtu.cn)

Abstract: Northeastern margin is a natural experimental field for studying crustal extrusion and expansion mechanism. Accurate crustal deformation pattern is a key point in the analysis of regional deformation mechanism and seismic hazard research and judgment. In this paper, the present-day GPS velocity field on the northeastern margin of the Tibetan Plateau was obtained from encrypted GPS observations around the Haiyuan-Liupanshan fault zone, combined with GPS observations on the northeastern margin of the Tibetan Plateau from 2010 to 2020. Firstly, we divided the study area into three relatively independent blocks: ORDOS block, Alxa block and Lanzhou block; secondly, the accurate fault distribution of the Haiyuan-Liupanshan fault zone was taken into account to obtain the optimal inversion model; finally, using the block and fault back-slip dislocation model, the inversion got the slip rate distribution, locking depth and slip deficit rate of each fault. The results indicate that the Laohushan Fault and Haiyuan Fault are dominated by left-lateral strike-slip, while the Liupanshan Fault is dominated by thrust dip-slip, and the Guguan-Baoji Fault has both left-lateral strike-slip and thrust dip-slip components. The maximum locking depths of the Laohushan Fault, Haiyuan Fault, Liupanshan Fault and Guguan-Baoji Fault are 5 km, 13 km, 15 km and 10 km respectively, and the locking of Haiyuan Fault is strong in the middle section and weak in the eastern and western section. The Haiyuan Fault is still in the post-earthquake stress adjustment stage. The slip deficit rate decays from 3.6 mm/yr to 1.8 mm/yr from west to east along the fault zone. Combined with geological and historical seismic data, the results suggest that the mid-long term seismic risk in the Liupanshan Fault is high.

Keywords: crustal deformation; Haiyuan-Liupanshan fault zone; slip rate; locking depth; slip deficit rate

1. Introduction

The northeastern margin of the Tibetan Plateau is the frontal region of the uplift development and expansion into the continental interior, the newest and forming part of the plateau, and a natural experimental field to study the continental interior deformation of China. The extrusion and deformation of the crust has resulted in the formation of complex tectonic zones and seismic activity zones, a series of historical earthquakes occurred on the active faults in the region and margins(Figure 1), such as the 1920 Haiyuan M8.5 earthquake and the 1927 Gulang M8.0 earthquake occurred on the HYF (Zhang et al., 1987) (Figure 1). According to the back-slip theory, a fault can accumulate strain accumulation near the fault surface due to the relative motion of the footwall and hangingwall blocks when the fault is locked, and produce a slip deficit phenomenon (Savage et al., 1983). Therefore, the quantitative study of the deformation and strain accumulation characteristics of the main faults in this region to achieve the precise crustal deformation patterns are the key for analyzing the mechanisms of regional deformation and assessing seismic hazards.

Many scholars have conducted large numbers of studies on this region by three methods: geological, GPS and InSAR. However, due to different spatial resolution of data, station density,

Preprints (www.preprints.org) | NOT PEER-REVIEWED | Posted: 17 April 2023 doi:10.20944/preprints202304.0378.v1

observation duration, and model selection, the slip rates and deformation characteristics show significant discrepancies (Table 1).

Table 1. Comparison of slip rate of four faults in different papers (Note: Slip rate unit is mm/yr, the LPSF is the dip-slip rate).

	Literature Sources	LHSF	HYF			LPSF		GGBJF
			Western	Middle	Eastern	Northern	Southern	
Geological results	Institute of Geology, National Seismological Bureau, 1990			3.3-9.2				
	Zhang et al., 1991	Zhongwei section: 8-10, Reduced eastward to 4-6						
	Burchfiel et al., 1991							
	Tian et al., 2001		5.8					
	Li et al., 2009		4.5±1.1					
Terrestrial measurement results	Wang et al., 2009		3.4±0.2					
	Hu et al., 2009	8.25	5.49		5.97			
	Cui et al., 2009	6.5	4.5	5.6	5.5			
	Duvall et al., 2010		2-4.5					
	Loveless et al., 2011		4.6-4.7					
	Zhang et al., 2011		2-5.5			1.0		
	Ge et al., 2013		2.9-5.9					
	Li Q. et al., 2013	5.4±0.1	5.0±0.1		5.0±0.2	1.3±0.1	1.7±0.1	
	Li et al., 2015		7.8-8.4			3.2		3.9
	Li et al., 2016	4.1±0.4	3.9±0.4	3.7±0.4	3.6±0.4	3.2±0.3	3.1±0.3	
	Ye et al., 2018		6.4	6.1	5.9	1.4	1.2	1.2
	Qiao et al., 2019	4.5-7.6		3.2-5.4				
	Xu et al., 2018	3.4±0.2		3.2±0.2		3.0±0.2		
	This article	3.5	3.2	3.0	3.1	1.9	1.8	1.3

In summary, the slip rates of the HYF obtained by geological methods are 3-10 mm/yr, with an average rate of 5-6 mm/yr; the slip rates of the HYF obtained derived from GPS observations and block deformation analysis are 2-9mm/yr; the slip rates of the LPSF are 1-3.5 mm/yr. Derived from InSAR technology, the average rate of the HYF is 3-5 mm/yr, and the LPSF is about 3 mm/yr.

In order to obtain a more accurate crustal deformation pattern of the faults on the northeastern corner of the Tibetan Plateau, this paper integrated the observations from encrypted GPS stations around the Haiyuan-Liupanshan fault zone, with the GPS observations on the northeastern margin of the Tibetan Plateau from 2010 to 2020, based on the block-fault back-slip dislocation model to obtain the locking depth, slip rate deficit distribution and motion characteristics of the faults.

2. Regional tectonic background

Preprints (www.preprints.org) | NOT PEER-REVIEWED | Posted: 17 April 2023 doi:10.20944/preprints202304.0378.v1

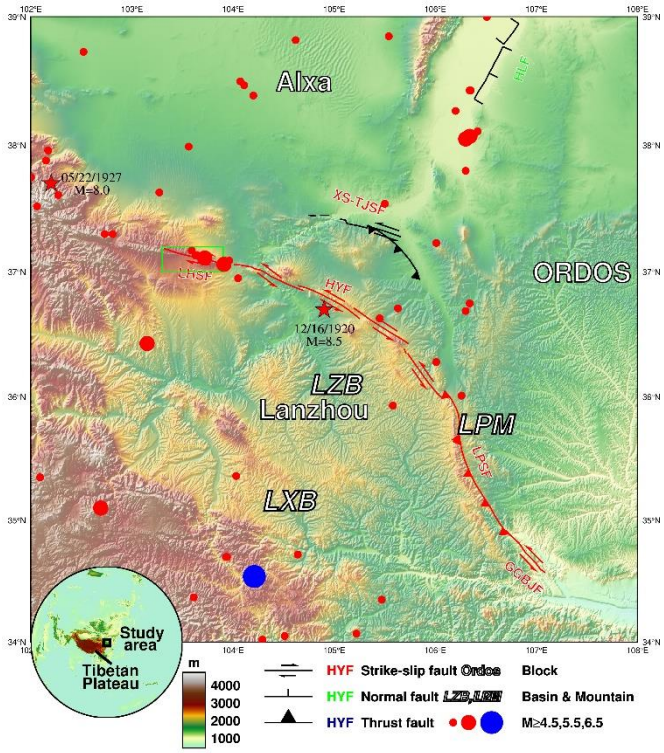

Figure 1. Tectonic background and distribution of faults on the northeastern margin of Tibetan Plateau. The red lines represent the Laohushan Fault (LHSF), Haiyuan Fault (HYF), Liupanshan Fault (LPSF) and Guguan-Baoji Fault (GGBJF). The black lines indicate other active faults in the region and marks the Xiangshan-Tianjingshan Fault, the Yellow River Fault; The red five-pointed stars indicate the epicenter positions of the Gulang M8.0 earthquake on May 22, 1927 and the Haiyuan M8.5 earthquake on December 16, 1920; The seismic data in the study area (indicate by red and blue circle) are from earthquakes with a magnitude of 4.5 or above in the center of China seismic network from January 1970 to January 2022.

The northeastern margin of the Tibetan Plateau is located on the plate that is extruded eastward by the collisional contraction between Indian and Eurasian plate at the orientation of at N20°E (Sella et al., 2002). Haiyuan-Liupanshan fault zone as a boundary fault zone on the northeastern corner of the Tibetan Plateau, which occupies a significant region for studying the mechanism of contraction and expansion of the Tibetan Plateau into the interior of Chinese continent (Deng et al., 1989). The HYF and LHSF are the junction faults between the Lanzhou and Alxa block, which is NWW trending with the top of the arc convex to NE (Figure 1), and its motion since the Late Cenozoic has been successively thrust and left-lateral strike-slip, and this strike-slip displacement has been absorbed by the LPSF to the east with east-west crustal shortening (Wang et al., 2014), and no earthquakes above magnitude 7 have gestated since 1920. The LPSF is a junction fault between the Lanzhou and ORDOS Block, with NNW trending and convex SW at the top of the arc (Figure 1), and is in the contraction tectonic area to the east of the HYF, which is a thrust fault and still has left-lateral strike-slip characteristics (Deng et al., 1989). Three magnitude 7 earthquakes occurred from 1200 to 1700 (Yuan et al., 2008), the earthquake risk should not be underestimated in the LPSF. The GGBJF is connected with the LPSF to the north and to the northern edge of the West Qinling Fault in the south, which trending NNW (Figure 1). It can be considered as the southern extension of the LPSF, but its movement pattern is completely different from that so its movement characteristics also deserve attention.

3. GPS observation data and block classification

3.1. GPS data and data processing

Preprints (www.preprints.org) | NOT PEER-REVIEWED | Posted: 17 April 2023 doi:10.20944/preprints202304.0378.v1

The GPS observations were obtained from the 2010-2020 data of the China Continental Environmental Tectonic Monitoring Network (CMONOC) on the northeastern margin of the Tibetan Plateau, which includes 260 continuous stations and 2000 active stations and was completed in 2009. To better constrain the near-field deformation of the HYF and LPSF, we set up eight continuous GPS stations with an average spacing of 20 km along the LPSF, along with two continuous GPS stations with a spacing of 10 km established along the Xiaokou Fault, which formed a new regional station network named the Seismic Forecasting Network (IEFNET) and has conducted nine periods of observations since April 2013. Richer GPS observations were used to obtain fault slip rate, and accurately capture the fault activity characteristics, and discuss the transition of Fault activity patterns in the intersection region of the HYF and LPSF. In addition, we have achieved other continuous GPS observations in this region derived from two other networks, partly from the Chinese Continental Environmental Tectonic Monitoring Network (CMONOC), the rest from a regional network (REGENT), which has been in operation since January 2010. Together with the encrypted GPS continuous observation stations we set up in the near-field of the LPSF, a total observation of 459 GPS stations were used in this study. The station distribution covers the main faults, with most stations located near major seismic zones, providing data assurance for obtaining a more accurate regional three-dimensional GNSS velocity field and data basis for obtaining a more accurate crustal deformation pattern in this region. GPS data solution strategy reference (Su et al., 2019). Figure 2 shows the GPS velocity field with respect to the Ordos block regional framework.

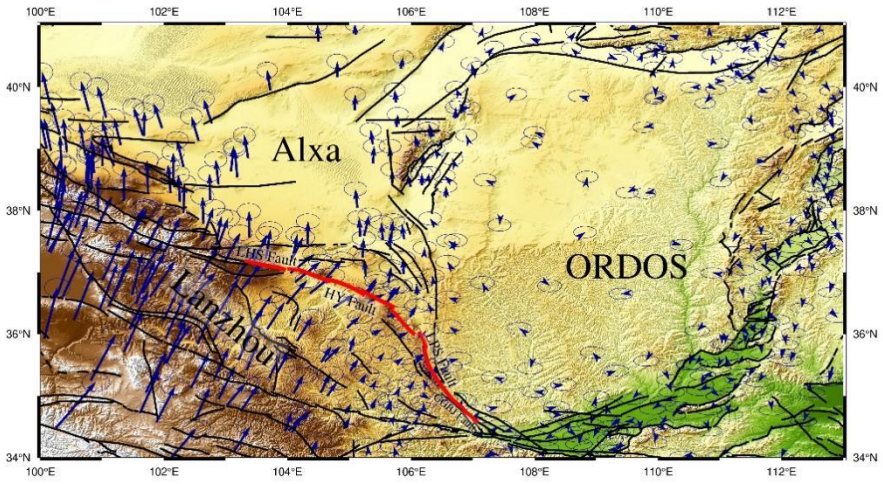

Figure 2. GPS velocity field of regional horizontal motion, with respect to ORDOS block.

3.2. Block division scheme

According to the previous division model of blocks (Zhang et al., 2003), the northeastern margin of the Tibetan Plateau is divided into the ORDOS block, Alxa block and Lanzhou block with the boundaries of the LHSF, HYF, LPSF and GGBJF, and block boundaries coincide with the active faults (Figure 3).

Preprints (www.preprints.org) | NOT PEER-REVIEWED | Posted: 17 April 2023 doi:10.20944/preprints202304.0378.v1

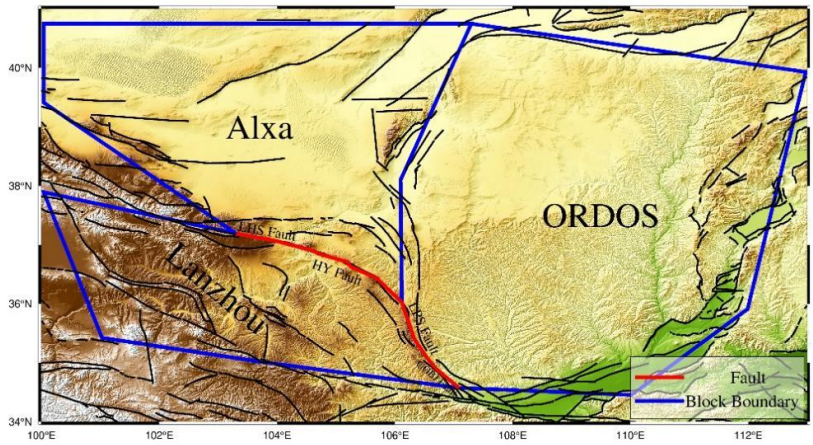

Figure 3. Block division scheme on the northeastern margin of the Tibetan Plateau. The red line indicates the faults studied in this paper; The blue line indicates the block boundary; The black lines indicate other faults in this area.

3.3. Fault geometry model

LHSF is the boundary between the Alxa and Lanzhou block, and intersects with the western section of the HYF; GGBJF is the boundary between the ORDOS and Lanzhou block, which is an extensional fault of LPSF and intersects the southern section of it. Both faults are highly active and have frequent historical earthquakes (Figure 1), which have a strong influence on the near-field observations of the Haiyuan-Liupanshan fault zone. In order to improve the accuracy of model inversion and better fit the GPS data, the two faults were added to the model and the elastic deformation caused by their locked was considered. The LHSF and HYF are the boundaries between the Alxa Block and Lanzhou Block, the LPSF and GGBJF are the boundary between the ORDOS Block and Lanzhou Block.

Accurate determination of the geometric model of the fault could make the model better fit the observed GPS velocity field, thus reducing the residuals of the velocity field to obtain better results. When modeling the fault surface (Figure 4), the dip angle of the LHSF and HYF was set to 60° with SSW tendency, and the dip angle of the LPSF and GGBJF was set to 45° with SW tendency. The fault was set to be completely locked (ϕ=1) at 0.1 km and free-slip (ϕ=0) below 25 km. The fault node parameterization type was set to one-dimensional depth profile type that node value is a function of depth (Wang et al., 2003), which was expounded in detail in Section 5.2. In the inversion, two surface nodes were set along the strike and six nodes were set along the depth direction for the LHSF, the HYF had 8 surface nodes and 6 depth nodes, the LPSF had 6 surface nodes and 6 depth nodes, the GGBJF had 3 surface nodes and 6 depth nodes.

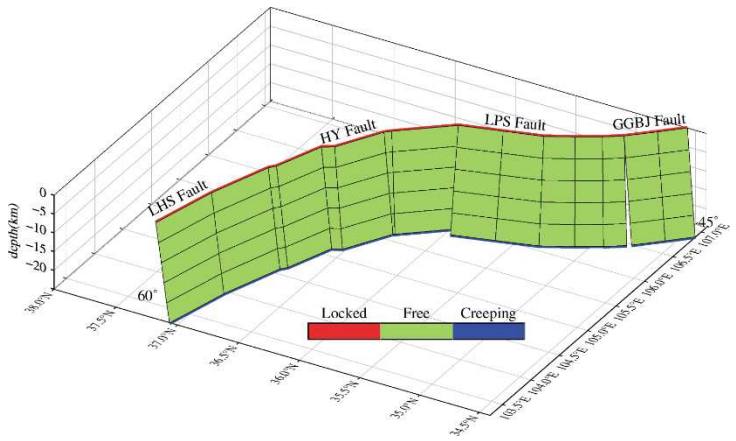

Figure 4. Simplified map and boundary conditions of faults model.

Preprints (www.preprints.org) | NOT PEER-REVIEWED | Posted: 17 April 2023 doi:10.20944/preprints202304.0378.v1

4. Inversion Principle

The model of interseismic deformation inversion of fault is block-fault back-slip dislocation model, which is calculated by TDEFNODE program. Constrained by the GPS velocity field, the model can obtain the block rigid motion parameters of the elastic lithosphere, the uniform strain rate inside the block and the surface elastic deformation caused by the fault locked at the block boundary by inversion (Savage et al., 1983; McCaffrey et al., 2007; McCaffrey, 2002; 2005). The rigid motion of the block is represented by the Euler pole, the uniform strain rate inside the block is represented by the spherical formula (Savage et al., 2001), and the slip deficit rate on the fault surface is based on the elastic half-space model (Okada et al., 1985). The detailed calculation formula is shown in (McCaffrey, 2002). One pure dynamical scalar ϕ is used to represent the degree of locking on the fault surface (McCaffrey, 2005; McCaffrey et al., 2007). The locking fraction ϕ has no unit, ϕ=0 indicates the fault is completely creeping, ϕ=1 indicates the fault is completely locked, and ϕ is between 0-1 indicates the fault is partially locked; its mathematical expression is $\phi = 1 - V_c/V$, V_c represents the short-term creep rate of the fault, and V represents the long-term slip rate of the fault. The fault geometry is represented by an irregular grid formed by three-dimensional nodes (longitude, latitude, depth) on the fault surface. The ϕ value of each node is calculated in the inversion. In order to obtain the linear change of ϕ value between adjacent nodes, the locking fraction of each divided sub-fault surface is obtained by bilinear interpolation. The slip deficit rate on the fault surface can be expressed by the product of the locking fraction ϕ and the long-term slip rate V.

The goodness of fit of the model to the observed data can be expressed by the chi-square value χ_n^2 (sum of chi-square / degree of freedom) (McCaffrey et al., 2007):

$$\chi_n^2 = \sum_{i=1}^{n} \left(\frac{r_i}{f\sigma_i}\right)^2 / f \tag{1}$$

In the formula, n is the number of observations, m is the number of parameters to be estimated, f is the degree of freedom; r_i is the residual errors of the observation, σ_i is the mean square error of the observation, and f is the weight of the observation. When χ_n^2 approaches 1, we considered that the model fits the observation data well. And the weighted root mean square error (W_{rms}), which is defined as (McCaffrey, 2002):

$$W_{rms} = \sqrt{\sum \frac{{r_i}^2}{(f\sigma_i)^2} / \sum \frac{1}{(f\sigma_i)^2}} \tag{2}$$

5. GPS data inversion results

5.1. Fault slip rate

The slip rate of the faults quantitatively describes the relative motion of the hangingwall and footwall blocks of the fault, which is of great significance for extracting the characteristics of the deformation field. The TDEFNODE uses the inversed block motion parameters to calculate the slip rate of the boundary fault (McCaffrey, 2004).

The slip rates of the LHSF, HYF, LPSF and GGBJF are shown in Table 1 and Table 2 and Figure 5. The results of the best-fit model indicate that the LHSF is dominated by left-lateral strike-slip with the rate of ~3.5 mm/yr, which is consistent with geology (Li et al., 2009) and geodesy (Wang et al., 2009; Duvall et al., 2010; Zhang et al., 2011; Ge et al., 2013; Xu et al., 2018), approaching with the result of 4.1 ± 0.4 mm/yr (Li et al., 2016). The HYF is dominated by left-lateral strike-slip with the rate of 2.8-3.3 mm/yr, and the average rate is about 3 mm/yr, which is close to the results of 3.3-9.2 mm/yr obtained by geology (Institute of Geology State Seismological Bureau, 1990) and 4.5 ± 1.1 mm/yr (Li et al., 2009), and is close to GPS, InSAR and other geodetic methods (Wang et al., 2009; Duvall et al., 2010; Zhang et al., 2011; Ge et al., 2013; Xu et al., 2018; Qiao et al., 2019), and is also consistent with the rates of 3.9 ± 0.4 mm/yr, 3.7 ± 0.4 mm/yr and 3.6 ± 0.4 mm/yr of the western, middle and eastern sections of the HYF (Li et al ., 2016). The average contraction rate is 0.6 mm/yr, and the maximum rate is 1.4 mm/yr in the middle of the fault. Overall, the slip rate of the HYF obtained by the geological method is 2-6.5 mm/yr (Tian et al., 2001; Yuan et al., 1998). Derived fromGPS, InSAR and other geodetic methods, the slip rate of the HYF obtained by different scholars using block model and

Preprints (www.preprints.org) | NOT PEER-REVIEWED | Posted: 17 April 2023 doi:10.20944/preprints202304.0378.v1

dislocation model is 1.2-9 mm/yr, our results are within the range of the above results. LPSF is dominated by thrust contraction with the rate of 1.7-1.9 mm/yr and slight left-lateral strike-slip with the rate of 0.1-0.9 mm/yr, which is close to the result of rates of 1.3 ± 0.1 mm/yr and 1.7 ± 0.1 mm/yr for the northern and southern sections obtained by (Li et al., 2013), and 1.4 mm/yr and 1.2 mm/yr (Ye et al., 2018). The GGBJF has both left-lateral strike-slip and thrust extrusion components. The strike-slip rate is 1.3-1.4 mm/yr and the contraction rate is 1.2-1.3 mm/yr, which is consistent with the result of (Ye et al., 2018).

Zhang et al. (1991) proposed that the total amount of left-lateral strike-slip component of the HYF should be balanced with the crustal shortening in the LPSF. Based on the inversion results of the model, there is a difference of about ~1 mm/yr. We speculate that this part of the differential motion may be converted into strain accumulation in this region. Li et al. (2014) and Li et al. (2015) suggested that the northern and southern segments of the LPSF both have the characteristics of thrust movement, and the thrust component of the northern is higher than the southern segment, which is consistent with our results.

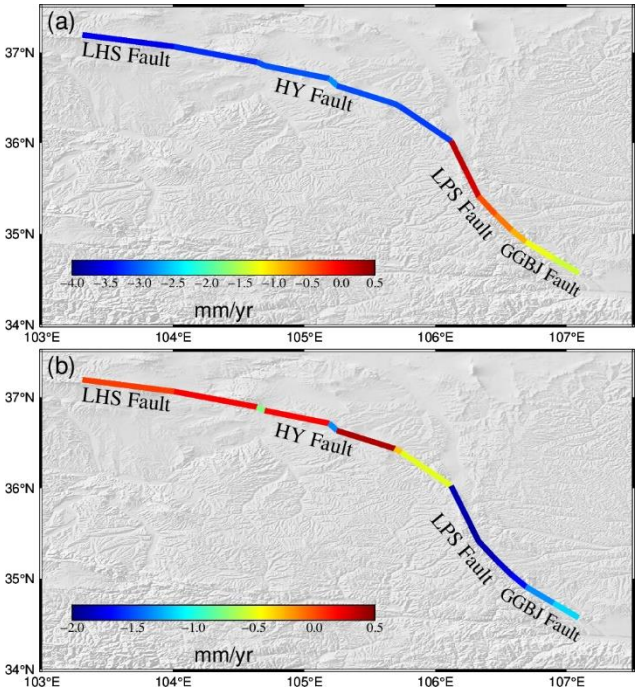

Figure 5. Fault slip rate. (a) is strike-slip component, positive value represents right-lateral strike-slip, while negative value represents left-lateral strike-slip; **(b)** is dip-slip component, positive value represents extension, and negative value represents contraction.

Table 2. Slip rate of each segment of the fault zone.

Fault name	Segment	Strike-slip rate（mm/yr）	Dip-slip rate（mm/yr）
LHSF		3.5	0.0
HYF	West	3.2	0.5
	Middle	3.0	0.8
	East	3.2	0.4
LPSF	North	0.3	1.9
	South	0.6	1.8
GGBJF		1.3	1.3

Preprints (www.preprints.org) | NOT PEER-REVIEWED | Posted: 17 April 2023 doi:10.20944/preprints202304.0378.v1

5.2. Fault locking slip distribution

According to fault geometry and optimal model results in section 2.3, the distribution of interseismic locking degree and slip deficit rate of each fault on the northeastern corner of the Tibetan Plateau were obtained (Figure 6, Figure 7, Table 3). From Figure 6, the locking degree of each fault is not uniformly distributed in the depth. The locking degree of LHSF is weak, the distribution is uniform and is strongest at the depth of 1 km, the maximum locking fraction is ~0.9, and decreases to 0.302 at the depth of 3~4 km, and is completely creep below the depth of 5 km. HYF is generally in the creep stage, but the locking degree is stronger than LHSF. The locking fraction of the western section gradually increases along the depth direction, and is strongest at the depth of 0-5 km, and gradually decreases below 5 km and is almost completely creep below 10 km. The eastern section exhibits the same behavior as the western. The locking in the middle is the strongest and evenly distributed with the depth of 7-8 km, and gradually decreases to the depth of 13 km, and is completely creep below 15 km. HYF had a magnitude 8.5 earthquake in 1920, and the focal depth is generally believed to be 17-20 km (Cui et al., 2009). Our results showed that the fault is still relatively weak at present. We considered that the fault is still in the post-earthquake adjustment stage under the influence of the earthquake, and its movement is still dominated by post-earthquake creep. In LPSF, the overall locking is the highest, with the southern section have stronger locking than the northern. The fault is completely locked within a depth of 5 km, and is still strongly locked within a depth of 10 km. The locking fraction decreases gradually at a depth of 10-15 km, and is completely creep below a depth of 15 km. Therefore, it is speculated that the fault may have a large strain accumulation. The locking fraction of GGBJF decreases gradually from the northern section to the southern section. The locking fraction is stronger when the depth is above 5 km, and gradually decreases between 5-10 km, and is completely creep below 10 km. Compared with previous studies, the locking depth of LPSF and GGBJF obtained in this paper is slightly lower, which may be related to different models and data, but the overall trend is consistent. The locking characteristics of each section of the fault zone will be discussed in detail in section 5.3.

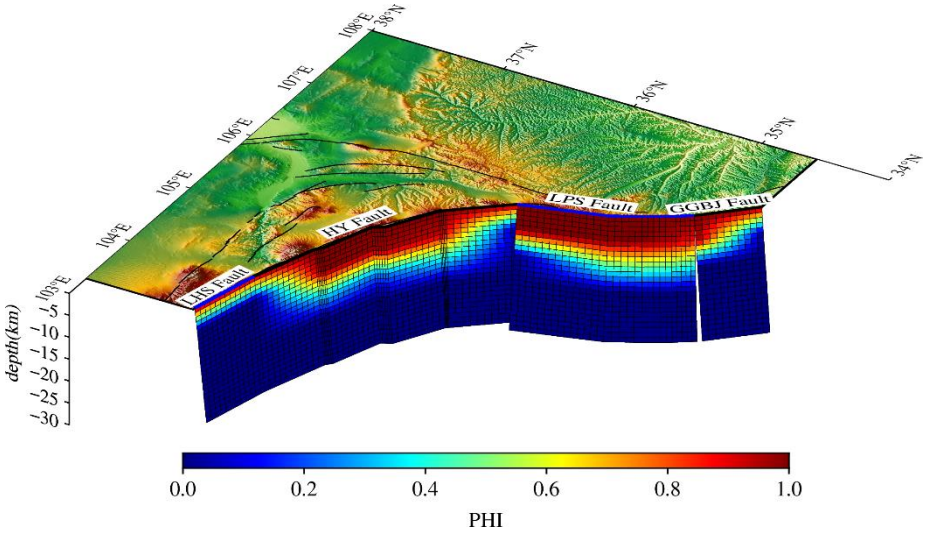

Figure 6. Locking degree of the Haiyuan-Liupanshan fault zone.

Preprints (www.preprints.org) | NOT PEER-REVIEWED | Posted: 17 April 2023 doi:10.20944/preprints202304.0378.v1

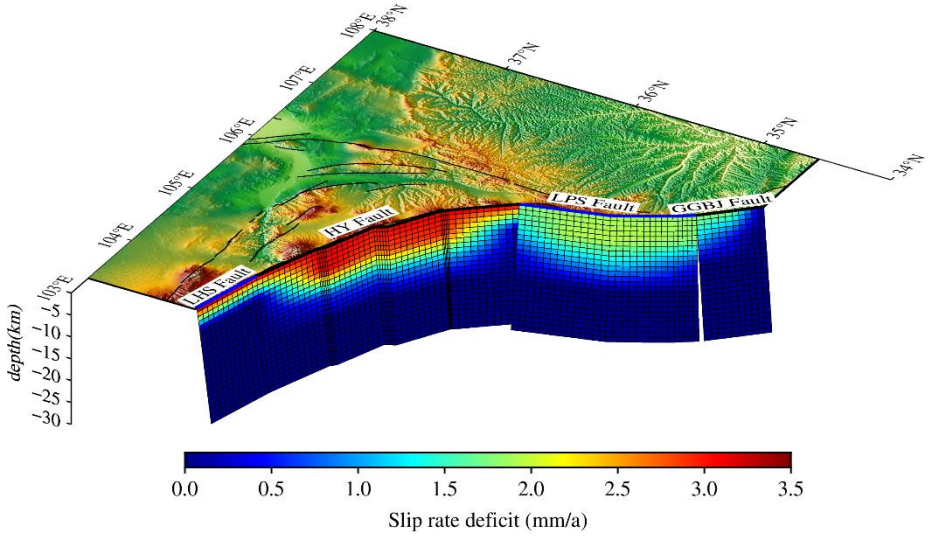

Figure 7. Slip deficit rate of the Haiyuan-Liupanshan fault zone.

Table 3. Slip rate, locking depth and slip deficit rate of each segament of the fault zone.

Fault name	Slip rate (mm/yr)	Locking depth (km)	Slip deficit rate (mm/yr)
LHSF	3.5	5	3.2-3.6
West section of HYF	3.2	10	2.8-3.2
Middle section of HYF	3.0	13	2.4-2.8
East section of HYF	3.2	10	~2.4
North section of LPSF	0.3	15	1.7-1.8
South section of LPSF	0.6	15	1.8-1.9
GGBJF	1.3	10	~1.8

Quantitative analysis of the strain accumulation on the fault surface is necessary to understand the seismic activity of the fault, which can be reflected by the locking degree of the fault, the stronger the locking degree, the easier the strain accumulation. The rate of strain accumulation can be quantitatively described by the slip deficit rate. The slip deficit rate could be calculated by the product of the fault long-term slip rate V and the locking fraction ϕ (McCaffrey et al., 2002). Figure 7 and Table 3 show the slip deficit rate distribution of faults.

For the same fault, the area where the slip deficit rate is significantly quick is the strongly locked region of the fault. The rate of slip deficit gradually decreases with depth along the fault surface until it reaches 0 mm/yr. This indicates that the fault surface no longer impedes the relative motion of the two blocks, and the fault is completely creep. McCaffrey et al. (2007) pointed out that " slip deficit rate " means that the energy not released by the long-term slip rate of the fault through creep slip is converted into strain energy to accumulate on the fault surface, so we used the slip deficit rate to quantitatively analyze the speed of strain accumulation on the fault surface. Similar to the distribution of the locking, the slip deficit rate of each fault is also unevenly distributed in depth, but the magnitude and trend of the slip deficit rate are similar to the locking distribution. The slip deficit rate decreased from 3.6 mm/yr at LHSF to 1.8 mm/yr at GGBJF. Figure 7 show that LHSF and HYF are mainly characterized by left-lateral slip deficit rate, among which the LHSF has the largest deficit rate with 3.6 mm/yr, but its depth is the shallowest, distributed from the surface to 5 km. The strike-slip deficit rate of the HYF is large with a maximum rate of 3.2 mm/yr, and the depth in the middle section is deepest, with the western section showing an increasing slip deficit rate with depth, while

Preprints (www.preprints.org) | NOT PEER-REVIEWED | Posted: 17 April 2023 doi:10.20944/preprints202304.0378.v1

the eastern section shows a decreasing rate towards the surface, with the distributed in a depth range from the surface to 15 km. LPSF is mainly dominated by the thrust dip-slip deficit rate with a maximum rate of 1.9 mm/yr, but its distribution depth of slip defict is relatively uniform, ranging from the surface to 15 km depth. GGBJF has both left-lateralstrike-slip and thrust dip-slip deficit rate. The rate gradually decreases from the northern to the southern segment with a maximum rate of 1.8 mm/yr, and is distributed within a depth range of 0-10 km.

5.3. Block motion

The optimal parameter model showed that the present model can better explain the surface GPS observations and obtain the rigid rotation parameters and internal strain parameters of the Alxa blocks and Lanzhou blocks. Figure 8 shows that the GPS velocity residuals of this model are randomly distributed and consistent with a gaussian distribution. Most of the residuals are within 1 mm and have a random direction. Some individual points have residuals between 2~3 mm, but they are far from the fault zone in this model, this may be due to the existence of active faults with strong activity in the area of larger residuals, such as the West Qinling Fault, which has no significant effect on the actual inversion results of this model. It indicates that the fitting degree between this model and GPS observation data is good and no obvious signals were missed.

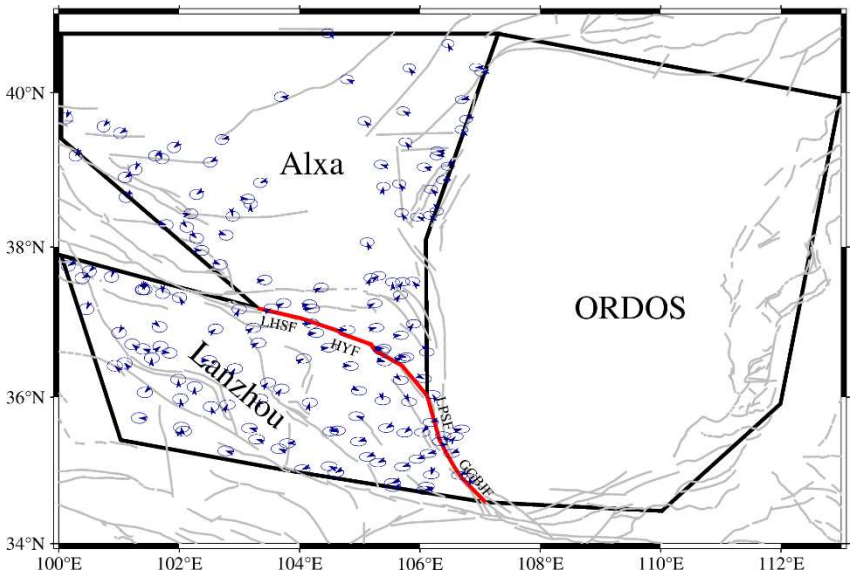

Figure 8. Residuals distribution of GPS velocity.

Since the ORDOS block is a rigid block, the model set it as the reference block without calculating its internal strain, so the motion of each block obtained is relative to the motion of the ORDOS block. The obtained rigid rotation parameters and internal strain parameters of each block are shown in Tables 4 and 5. Relative to the ORDOS block, both the Alxa block and the Lanzhou block make clockwise rotation, and the former has a larger rotation rate than the latter. The Euler pole of the Alxa block is far from the block itself and located on the northeastern of the ORDOS block; the Euler pole of the Lanzhou block is far from the inner part of the block and located on the south of the ORDOS block. The motion trend of the block is consistent with the collision of the Indian plate in the N20 ° E direction (Sella et al., 2002) with the Eurasian plate, resulting in an eastward extrusion of the northeastern margin of the Tibetan Plateau. However, when the relatively stable ORDOS block is encountered, the movement direction is deflected to the south, showing a characteristic of clockwise movement along the fault zone. Compared with the relatively stable Alxa block, the internal strain rate of Lanzhou block is larger and dominated by compressive strain, supplemented by tensile strain, which is due to the lateral escape of the crust blocked by the relatively stable Alxa block and the hard ORDOS block (Meyer et al., 1998), the principal compressive strain rate $\dot{\varepsilon}_1$=14.34 nanostrain/yr , and the tensile strain rate $\dot{\varepsilon}_2$=6.05 ns/yr. Compared with the results of previous studies, the magnitude of

Preprints (www.preprints.org) | NOT PEER-REVIEWED | Posted: 17 April 2023 doi:10.20944/preprints202304.0378.v1

the kinematic parameters of the blocks differs due to the different block divisions, but the kinematic trend of the block is consistent (Wang et al., 2003; Hao et al., 2017; Li et al., 2014).

Table 4. Euler parameters and internal strain rate of each block, relative to the ORDOS block. The angular velocity of rigid body. rotation is positive with counterclockwise rotation.

Block name	Eulerian vector			Internal strain rate (nanostrain/yr)		
	$\Lambda(°)$	$\Phi(°)$	$\Omega(°/Ma)$	$\dot{\varepsilon}_1$	$\dot{\varepsilon}_2$	$A(°)$
Alxa Block	110.4658	39.0087	-0.4106	-5.10	4.46	28.18
Lanzhou block	110.3636	32.0201	-0.3731	-14.34	6.05	50.04

Table 5. Internal uniform strain tensor of each block.

Block name	Internal strain rate (nanostrain/yr)		
	ε_{xx}	ε_{yy}	ε_{xy}
Alxa Block	2.33	-2.96	-3.98
Lanzhou block	-5.93	-2.36	-10.04

6. Discussion

6.1. Comparison of modeling results for different fault participation

In order to verify whether adding LHSF and GGBJF to the model improved the data fitting degree, four sets of experiments were done for comparison, in the first group, HYF and LPSF were modeled; in the second group, LHSF, HYF and LPSF were modeled; in the third group, HYF, LPSF and GGBJF were modeled. In the fourth group, LHSF, HYF, LPSF and GGBJF were modeled and analyzed. When modeling the faults, only the motion of the surrounding circumscribed blocks was considered, and only the data within the corresponding blocks were used, while kept the other model parameters unchanged. The modeling results are shown in Table 6.

Table 6. Comparison of modeling results of different faults.

Number	Faults in modeling	Used date	Blocks	χ_n^2	W_{rms} of Alxa Block	W_{rms} of Lanzhou block
1	HYF, LPSF	526 stations	ORDOS, Alxa, Lanzhou	1.633	0.629	0.892
2	LHSF, HYF, LPSF	538 stations	ORDOS, Alxa, Lanzhou	1.599	0.589	0.872

3	HYF, LPSF, GGBJF	542 stations	ORDOS, Alxa, Lanzhou	1.591	0.652	0.845
4	LHSF, HYF, LPSF, GGBJF	554 stations	ORDOS, Alxa, Lanzhou	1.534	0.613	0.784

The result shows that the addition of LHSF and GGBJF can improve the overall fitting effect of the GPS observations, reducing both χ_n^2 and the W_{rms} of the data within the Alxa and Lanzhou blocks. The effect of adding GGBJF in the experiment is slightly greater than that of LHSF, which may be due to the existence of shallow creep near LHSF and the greater activity of GGBJF, as well as the more abundant near-field data. When modelled the fault zone, both LHSF and GGBJF were added in the inversion finally.

6.2. Optimal model parameters setting

Parameters setting in the model mainly include, selecting reference block, block properties (rigid or elastic), fault parameterization type, limit of locking depth, and constructing fault (node, fault slip type, locking depth, fault dip angle, node index) and making pseudo-fault (closure block), etc. The locking depth is the depth at which the fault slip completely freely, and the locking depth was set to 25 km in this model. Previous research showed that the ORDOS block is stable and rigid, so the ORDOS block was set as the reference block in the inversion, and its internal strain was not calculated. Lanzhou block and Alxa block were set as elastic blocks and their internal strains were calculated. The geometrical characteristics of faults had been studied extensively, and some results on the dip angle of major faults are given in Table 7. The dip angles of LHSF and HYF are between 41° and 70°, and the optimal dip angle was 60° by grid search; the dip angle of LPSF is between 20° and 70°, and the optimal dip angle was 45° by grid search; the dip angle of GGBJF is between 45° and 88°, and the optimal dip angle was 45° by grid search.

Table 7. Fault dip angles of the Haiyuan-Liupanshan fault zone.

Fault name	Fault dip angle
LHSF	65° (Li et al., 2016); 60° (Ye et al., 2018); 70° (Hao et al., 2017)
HYF	75° (Li et al., 2014); 50° (Zhao et al., 2016); 40°~60° (Zhang et al., 2005); 65° (Li et al., 2016); 60° (Ye et al., 2018); 70° (Hao et al., 2017)
LPSF	45° (Li et al., 2014; Hao et al., 2017; Ye et al., 2018; Li et al., 2016); 20°~70° (Zhang et al., 2005); 35°~55° (Hao et al., 2017)
GGBJF	45° (Wan et al., 2009); 55°~88° (Shi et al., 2011)

The initial locking depths of the faults can also be calculated by grid search. For LHSF and HYF, the initial locking depth is 15 km by searching in the range of 10 km-20 km, for LPSF and GGBJF, the initial locking depth is 15 km by searching in the range of 15 km-25 km. With other parameters unchanged, the model performed inversion at intervals of 5km at locking depths between 15km and 40 km. Comparing the χ_n^2 of the results, it was concluded that 25 km was the optimal choice for this model. In addition, according to the catalogue of earthquakes above M3-magnitude in mainland China and its surrounding areas (Xu et al., 2014) and the study on precise location of earthquakes

Preprints (www.preprints.org) | NOT PEER-REVIEWED | Posted: 17 April 2023 doi:10.20944/preprints202304.0378.v1

(Yang et al., 2005) both showed that the focal depth of most earthquakes on the northeastern margin of the Tibetan Plateau is less than 25 km. Therefore, the final locking depth was set as 25 km.

The fault node settings were given in Section 2.3. The locking fraction between 0.1 km and 25 km were inverted by block-fault back-slip dislocation model ($0 \leq \phi \leq 1$), and the fault locking fraction was set in the way of (Wang et al., 2003), setting the node ϕ values as a function of depth, expressed as follows.

$$G' = 20.0 - G \qquad (10.0 \leq G \leq 20.0)$$

$$\phi(z) = 1.0 \qquad (z \leq Z1)$$

$$\phi(z) = \frac{\exp(-z'/G' - \exp(-1.0/G'))}{1.0 - \exp(-1.0/G')} \qquad (Z1 < z < Z2) \qquad (3)$$

$$\text{Which } z' = (z - Z1) / (z - Z2)$$

$$\phi(z) = 1.0 \qquad (z \geq Z2)$$

In formula (3), G is the shape parameter that constrains the decay of the locking fraction, Z1 is the upper boundary of the transition region, the depth where the fault is completely locked, and Z2 is the lower boundary of the transition region, the depth where the fault slips freely. When $z \leq Z1$, the fault is completely locked; when $z \geq Z2$, the fault is completely creep-slip; in $Z1 < z < Z2$, the locking fraction of the fault node decays as a function of formula (3).

6.3. Distribution characteristics of the degree of locking and slip deficit rate in different segments of the fault zone

The results show that LHSF and HYF are dominated by left-lateral strike-slip, LPSF is dominated by thrust dip-slip, and GGBJF has both component of left-lateral strike-slip and thrust dip-slip. As shown in Figure 6 and Figure 7, the locking in the LHSF is uniformly distributed, with a strong locking within 1 km, followed by a gradual decay of the locking fraction to a complete creep slip below 5 km and with a slip deficit rate of 3.4 mm/yr, which is consistent with the results of (Yuan et al., 1998; Li et al., 2015; Ye et al., 2018). The 1920 Haiyuan 8.5 magnitude earthquake on HYF formed a 200 km long left-lateral strike-slip rupture zone at the surface (Zhang et al., 1987). The overall HYF is in the creep-slip stage, with an overall locking depth of 15 km, but the locking fraction at the depth of 13-15 km is quite small, so the locking depth is considered to be 13 km. The locking of the western section is weak, with locking fraction gradually increases along the strike, and is strong within 5 km, gradually decaying to the depth of 10 km, the slip deficit rate is 2.8-3.2 mm/yr. The middle section has the strongest locking and relatively uniform distribution with the depth reaches 7-8 km, then gradually decays to 13 km and completely creep below 13km, its slip deficit rate is 2.4-2.8 mm/yr; the east section has the same expression as the western, except that its locking fraction gradually decays in depth along the strike, and the slip deficit rate is ~2.4 mm/yr. In summary, the locking of HYF is similar to the arc-shaped distribution (Figure 6) with a characteristic of weak locking in the west and east sections and strong locking in the middle section, and the slip deficit rate decreases from 3.2 mm/yr to 2.4 mm/yr from west to east. In general, the strain accumulation capacity of the HYF is relatively low. Combining the earthquake recurrence interval is 800-1600 years (Zhang et al., 1987) and the focal depth is generally considered to be 17-20 km, so we considered that HYF is still in the post-earthquake stress adjustment stage, which better explains the absence of earthquakes of magnitude 6.0 or higher in this fault since 1920. The locking of the LPSF is overall the strongest and evenly distributed, with slightly higher locking in the southern section compared to the northern. The high-value locking fraction areas are distributed almost across the entire fault surface within 10 km (Figure 6), the fault is completely locked within 5 km depth (ϕ=1), and strong locking fraction ($\phi \geq 0.5$) still exists within 5-10 km and gradually decreases at 10-15 km, and is completely creep below 15 km depth; the overall slip deficit rate is 1.7-1.9 mm/yr, reflecting the characteristic that the southern section is higher than the northern. The overall locking of GGBJF is weak, and the locking fraction gradually decreases along the strike at depth, with the strongest locking near the southern section of LPSF, where the locking degree is strong in 5 km, and gradually decreases to 10 km in depth and completely creep; its slip deficit rate decreases from 1.8 mm/yr to 0.2 mm/yr from west to east. The

north-south segmented movement characteristics of the LPSF are clearly evident (Hao et al., 2014). Which the southern section of the LPSF refers to the GGBJF in this study, in this way, the results of this paper show that the north-south section of LPSF has obvious motion characteristics, and the north section is more active than the south section. In terms of the locking degree, LPSF is easier to strain accumulation, but in terms of the slip deficit rate, it accumulates strain slowly; however, no earthquake of magnitude 7.0 or higher has occurred on LPSF in the past 1400 years (Working Group of M7, 2012), so it will still reach high strain accumulation after long-term accumulation, which will lead to a strong earthquake, such as the Wenchuan earthquake.

The results also found that there was a weak right-lateral strike-slip phenomenon with the rate of 0.1-0.2 mm/yr in the top area of the HYF when it was converted from the sinistral strike-slip region at the tail end of the eastern segment to the northern segment of the LPSF. If we consider the explanation of this phenomenon, we believe that this area is located on the junction transition area of three blocks, while Alxa block and Lanzhou block are rotating clockwise around the ORDOS block, Lanzhou block is also rotating clockwise slightly around Alxa block. However, due to the obstruction of the hard ORDOS rigid block to the east, the motion of the block boundary in the transitional area changes, resulting in a right-lateral strike-slip phenomenon. There is another explanation, the displacement along a strike-slip fault must be absorbed and adjusted at a certain part along the fault, often at both ends of the fault, so that the whole fault can reach a new balance in energy, the contraction structure at the end of HYF is this kind of tectonic deformation (Deng et al., 1989). Therefore, we can also assume that the energy accumulated by the left-lateral strike-slip at the end of HYF may be released by the right-lateral strike-slip at the top of the northern section of LPSF to achieve a relative energy balance. Secondly, the phenomenon of weak left-lateral extension in some segments of HYF in our results can also be explained by this theory.

7. Conclusions

In this paper, we gathered the observations of encrypted GPS stations around Haiyuan-Liupanshan fault zone, integrated the GPS velocity field of the northeastern margin of the Tibetan Plateau and neighboring areas from 2010 to 2020, and obtained the present-day GPS velocity field of the northeastern margin of the Tibetan Plateau. We divided the region around the fault zone into independent blocks, taking into account the fine fault distribution of the Haiyuan-Liupanshan fault zone to obtain the optimal inversion model. A block-fault back-slip dislocation model is used to invert the slip rate, locking depth and the slip deficit rate of the faults. Combining the results of historical seismic data, regional geological data, and the motion characteristics of each fault, we discussed and analyzed the locking degree and slip deficit rate distribution characteristics of different segments of the fault zone. The main conclusions are as follows.

(1) LHSF is mainly controlled by left-lateral strike-slip with a rate of ~3.5mm/yr. The fault is in a completely locked within 1 km in depth, and is completely creep below 5 km, so the locking degree of this fault is low. Combined with the slip deficit rate of 3.2-3.6 mm/yr, we considered that the seismic risk of this fault is low.

(2) HYF is mainly controlled by left-lateral strike-slip with a rate of 3.0-3.2 mm/yr. The western and eastern sections of the fault are weakly locked, with strong locking at a depth of 5 km, and complete creep at a depth of 10km or less. The whole fault is completely creep below 13 km, and the overall locking degree showed the distribution characteristics of strong in the middle section and weak in eastern and western. Combined with the slip deficit rate of 2.4-3.2 mm/yr, we believe that there is a certain amount of strain accumulation in the middle section, but combined with the regional geological and historical seismic data, we believe that this fault is still in the post-earthquake stress adjustment stage, the seismic risk is considered low.

(3) LPSF is mainly controlled by thrust dip-slip with a rate of 1.7-1.9 mm/yr. The overall degree of locking in this fault is the strongest and uniformly distributed, and is completely locked at a depth of 5 km, and there is still strong locking at a depth of 10 km, and the fault is completely creep at a depth of 15 km or less; the slip deficit rate of this fault is 1.7-1.9 mm/yr. Although its rate of strain accumulation is slow, combining the analysis of geology, historical seismic data and the activity

characteristics, there is still a risk of mid to strong earthquake after a long period of strain accumulation, which should be continuously observed and analyzed.

(4) GGBJF has both left-lateral strike-slip and thrust dip-slip components, its strike-slip rate is 1.3-1.4 mm/yr and dip-slip rate is 1.2-1.3 mm/yr, the locking fraction decreases gradually from north to south, the locking is strong in the range of 5 km in depth, and is completely creep below 10 km, combined with its slip deficit rate of 1.8 mm/yr decay to 0.2 mm/yr from west to east. The seismic risk of this fault is considered to be low.

Author Contributions: Conceptualization, S.Y. and X.S.; methodology, S.Y. and X.S.; validation, S.Y. and X.S.; formal analysis, S.Y.; resources, S.Y. and X.S.; data curation, S.Y. and X.S.; writing—original draft preparation, S.Y.; writing—review and editing, X.S.; supervision, X.S.; project administration, X.S.; funding acquisition, X.S. All authors have read and agreed to the published version of the manuscript.

Funding: This research was funded by the National Natural Science Foundation of China (42174003), Gansu Province Science and Technology Association, Gansu Province Youth Talent Lifting Project (GXH20210611-06), Gansu Province Outstanding Youth Fundation (22JR5RA315), Lanzhou Jiaotong University, Youth Science Foundation Project (2021003).

Acknowledgments: The authors would like to thank the editors and anonymous reviewers for their detailed and constructive comments, which helped to significantly improve the manuscript.

Conflicts of Interest: The authors declare no conflict of interest.

References

Cavalié, O.; Lasserre, C.; Doin, M.P. Measurement of interseismic strain across the Haiyuan fault (Gansu, China), by InSAR.J. Earth and Planetary Science Letters. 2008, 275(3-4):246–257. https://doi.org/10.1016/j.epsl.2008.07.057.

Cui, D.X.; Hu, Y.X.; Wang, W.P.; Zhu,G.Z. Coulomb Stress Accumulation along Haiyuan Fault Zone. J. Earth Science-Journal of China University of Geosciences. 2009, 34(04):641-650. https://kns.cnki.net/kcms/detail/detail.aspx?FileName=DQKX200904011&DbName=CJFQ2009.

Deng, Q.; Chen S.; Song, F. Variations in the Geometry and Amount of Slip on the Haiyuan (Nanxihaushan) Fault Zone, China and the Surface Rupture of the 1920 Haiyuan Earthquake. J. Earthquake Source Mechanics. 2014, 29(2):264-266. https://doi.org/10.1029/GM037p0169.

Deng, Q.D.; Zhang, W.Q.; Zhang, P.Z. Haiyuan strike-slip fault zone and its compressional structures of the end. J. Seismology and Geology. 1989, 11(1):1-14(in Chinese). https://doi.org/10.3321/j.issn:1006-9267.2002.12.007.

Duvall, A.R.; Clark, M.K. Dissipation of fast strike-slip faulting within and beyond northeastern Tibet. J. Geology. 2010,38(3):223-226. https://doi.org/10.1130/G30711.1.

Fukuda, J.; Johnson, K.M. New methods for estimating the spatial distribution of locked asperities and stress-driven interseismic creep on faults with application to the San Francisco Bay Area, California. 2010. Journal of Geophysical Research:SolidEarth, 115:B12408. https://doi.org/10.1029/2010JB007703.

Gan, W.J.; Zhang, P.Z.; Shen, Z.K. Present-day crustal motion within the Tibetan Plateau inferred from GPS measurements. J. Journal of Geophysical Research. 2007, 112(B8):1-14. https://doi.org/10.1029/2005JB004120.

Ge, W.P.; Wang, M.; Shen, Z.K.; Yuan, D.Y.; Zheng, W.J. Intersiesmic kinematics and deformation patterns on the upper crust of Qaidam-Qilianshan block.Chinese. J. Geophys. (in Chinese). 2013, 56(09):2994-3010. https://doi.org/10.6038/cjg20130913.

Hao, M.; Li, Y.H.; Qin, S.L. Spatial and Temporal Distribution of Slip Rate Deficit Across Haiyuan-Liupannshan Fault Zone Constrained by GPS Data. J. SEISMOLOGY AND GEOLOGY. 2017, 39(03):471-484. https://doi.org/10.3969/j.issn.0253-4967.2017.03.003.

Hao, M.; Wang, Q.L.; Shen, Z.K. Present-day crustal vertical movement inferred from precise leveling data in eastern margin of Tibetan plateau. J. 2014, Tectonophysics,632:281-292. https://doi.org/10.1016/j.tecto.2014.06.016.

Hu, Y.X.; Cui D.X.; Zhang, X.; Wang, X. Inversion and Analysis on the Active Characteristics of Subsections of Haiyuan Fault Belt Using GPS Data. J. Northwestern Seismological Journal. 2009, 31(03):227-230+253. https://kns.cnki.net/kcms/detail/detail.aspx?FileName=ZBDZ200903004&DbName=CJFQ2009.

Institute of Geology, China Earthquake Administration, Ningxia Earthquake Administration. Haiyuan Active Fault Zone (in Chinese). M. 1990. Seismological Press, Beijing.

Jolivet, R.; Lasserre, C.; Doin, M.P. Shallow creep on the Haiyuan fault (Lanzhou, China) revealed by SAR interferometry. J.Journal of Geophysical Research: Solid Earth (1978–2012). 2012, 117(B6):137-147. https://doi.org/10.1029/2011JB008732.

Jolivet, R.; Lasserre, C.; Doin, M.P. Spatio-temporal evolution of aseismic slip along the Haiyuan fault, China: implications for fault frictional properties. J. Earth and Planetary Science Letters. 2013, 377-378(5):23-33. https://doi.org/10.1016/j.epsl.2013.07.020.

Li, C.Y.; Zhang, P.Z.; Yin, J.H. Late Quaternary left-lateral slip rate of the Haiyuan Fault, northeastern margin of the Tibetan plateau. J. 2009, Tectonics,28(5):TC5010. https://doi.org/10.1029/2008TC002302.

Li, Y.C. et al., Fault locking and slip rate deficit of the Haiyuan-Liupanshan fault zone in the northeastern margin of the Tibetan Plateau. J. Geodyn. 2016. http://dx.doi.org/10.1016/j.jog.2016.07.005.

Li, Y.C.; Qu, C.Y.; Shan, X.J. Deformation of the Haiyuan-Liupanshan fault zone inferred from the denser GPS observations.J. Earthquake Science. 2015, 28(5-6):319-331. https://doi.org/10.1007/s11589-015-0134-z.

Li, Q.; Jiang, Z.S.; Wu, Y.Q.; Zhao, J.; Wei, W.X.; Liu, X.X. Present-day tectonic deformation characteristics of Haiyuan-Liupanshan fault zone. Journal of Geodesy and Geodynamics. J. 2013, 33(02):18-22. http://dx.doi.org/10.14075/j.jgg.2013.02.030.

Li, Q.; Jiang, Z.S.; Wu. Y.Q.; Zhao, J. Inversion of Locking and Distribution of Slip Deficit in Haiyuan-Liupanshan Fault Zone Using GPS Data. J. Geomatics and Information Science of Wuhan University. 2014., 39(05):575-580. http://dx.doi.org/10.13203/j.whugis20120161.

Li, Y.H.; Cui, D.X.; Hao, M. GPS-Constrained Inversion of Slip Rate on Major Active Faults in the Northeastern Margin of Tibet Plateau. J. Earth Science-Journal of China University Geosciences. 2015, 40(10):1767-1780. http://dx.doi.org/10.3799/dqkx.2015.158.

Loveless, J.P.; Meade, B.J. Partitioning of localized and diffuse deformation in the Tibetan Plateau from joint inversions of geologic and geodetic observations. J. Earth and Planetary Science Letters. 2011, 303(1-2):11-24. https://doi.org/10.1016/j.epsl.2010.12.014.

Meyer, B.; Tapponnier, P.; Bourjot, L. Crustal thickening in Gansu-Qinghai, lithospheric mantle subduction, and oblique, strike-slip controlled growth of the Tibet Plateau. J. Geophysical Journal International. 1998, 135:1-47. https://doi.org/10.1046/j.1365-246X.1998.00567.x.

McCaffrey, R. Block kinematics of the pacific–north America plate boundary in the southwestern United States from inversion of GPS, seismological, and geologic data. J. Journal of Geophysical Research. 2005, 110(B7):1-25. https://doi.org/10.1029/2004JB003307.

McCaffrey, R. Crustal block rotations and plate coupling. C. Stein S，Freymueller J T. Plate Boundary Zones. 2002, AGU, Washington DC:101-122. https://doi.org/10.1029/GD030p0101.

McCaffrey, R.; Qamar, A.I.; King, R.W. Fault locking, block rotation and crustal deformation in the Pacific Northwest. J. Geophysical Journal International. 2007, 169(3):1315-1340. https://doi.org/10.1111/j.1365-246X.2007.03371.x.

Okada, Y. Surface deformation due to shear and tensile faults in a half-space. J. Bulletin of the Seismological Society of America. 1985, 75(4):1135-1154. https://doi.org/10.1785/BSSA0750041135.

Qiao, X.; Qu, C.Y.; Shan, X.J.; Li, Y.C.; Zhu, C.H. Deformation Characteristics and kinematic Parameters Inversion of Haiyuan Fault Zone Based on Time Series InSAR. J. Seismology Mology and Geology. 2019, 41(06):1481-1496. http://dx.doi.org/10.3969 /j.issn.0253-4967.2019.06.011.

Qu, C.Y.; Shan, X.J.; Xu X.W. Near-field motion of the Haiyuan fault zone in the northeastern margin of the Tibetan Plateau derived from InSAR permanent scatters analysis. J. Journal of Applied Remote Sensing. 2013, 7(18):6451-6465. https://doi.org/10.1117/1.JRS.7.073507.

Savage, J.C.; Prescott, W.H. Asthenosphere readjustment and the earthquake cycle. Journal of Geophysical Research: Solid Earth. 1978, 83(B7):3369-3376. https://doi.org/10.1029/JB083iB07p03369.

Savage, J.C. Dislocation model of strain accumulation and release at a subduction zone. J. Journal of Geophysical Research Atmospheres. 1983, 88(B6):4984-4996. https://doi.org/doi:10.1029/jb088ib06p04984.

Savage, J.C.; Gan, W.; Svarc, J.L. Strain accumulation and rotation in the Eastern California Shear Zone. J. Journal of Geophysical Research Solid Earth. 2001, 106(B10):21995-22007. https://doi.org/10.1029/2000JB000127.

Sella, G.F.; Dixon, T.H.; Mao, A. A model for recent plate velocities from space geodesy. J. Journal of Geophysical Research:Solid Earth. 2002, 107(B4):2081-2091. https://doi.org/10.1029/2000JB000033.

Shi, W. The Analysis of the Developmental characteristics and Activity about Fault zone of Longxian-Baoji. Chang an University.2011. https://kns.cnki.net/kcms2/article/abstract?v=2OF-LjPvQ9cFh1umQjfhDTBaw1FnlZyyQSXGbPPGumAtXPtDIGPvggWEGTC5THc7Y-WbtRDiqQDYk1vBcmm3lj39hg_t9QrTMsXd_vJs0ebFMNHYbZ8RTg==&uniplatform=NZKPT&language=CHS.

Shi, Z.G. The recent activity features of faults and risk trend of strong earthquake in Liupanshan region. Lanzhou Institute of Seismology(China). 2011. https://kns.cnki.net/KCMS/detail/detail.aspx?dbname=CMFD201402&filename=1014240181.nh.

Su, X.N.; Yao, L.B.; Wu, W.W.; Meng, G.J.; Su, L.N.; Xiong, R.W.; Hong, S.Y.; Crustal Deformation on the Northeastern Margin of the Tibetan Plateau from Continuous GPS Observations. J. Remote Sens. 2019, 11(1), 34. https://doi.org/rs11010034.

Tian, Q.J.; Ding, G.Y.; Shen, X.H. Pull-apart Basins and the Totel Lateral Displacement along the Haiyuan Fault Zone in Cenozoic. J. EARTHQUAKE RESEARCH IN CHINA. 2001, (02):67-75. http://dx.doi.org/10.3969/j.issn.1001-4683.2001.02.007.

Wang, W.; Yang, S.; Wang, Q. Crustal block rotations in Chinese mainland revealed by GPS measurements. J. Earthquake Science. 2009, 22(6):639-649. https://doi.org/10.1007/s11589-009-0639-4.

Wang, W.T.; Zhang, P.Z.; Zheng, D.W.; Pang, J.Z. Late Cenozoic tectonic deformation of the Haiyuan fault zone in the northeastern margin of the Tibetan Plateau. J. Earth Science Frontiers. 2014,21(04):266-274. http://dx.doi.org/10.13745/j.esf.2014.04.027.

Wan, Y.G.; Shen, Z.K.; Sheng, S.Z.; Xu, X.F. The influence of 2008 Wenchuan earthquake on surrounding faults. J. Acta seismologica Sinica. 2009, 31(02):128-139. https://kns.cnki.net/kcms2/article/abstract?v=2OF-LjPvQ9eKuVkTgByJqbqBWmlnkjxJJDGs7mn47PGNiT_Iw8jEwCkr1Y25xQ_3cwmFszdefsuL_VtMZr5AnIIPbtC064G1KUzuPUjNPqxM9EOcj0rAqA==&uniplatform=NZKPT&language=CHS.

Wang, Y.P.; Shen, J.; Wang, Q. On the lateral contraction of Sichuan-Yunnan block (Chuandian block). J. Earth Science Frontiers (in Chinese). 2003, 10(Z1):188-192.

Wang, K.; Wells, R.; Mazzotti, S. A revised dislocation model of interseismic deformation of the Cascadia subduction zone. J. Journal of Geophysical Research Atmospheres. 2003, 108(B1):327-327. https://doi.org/10.1029/2001JB001227.

Working Group of M7. Study on the Mid-to Long-Term Potential of Large Earthquakes on the Chinese Continent. M. Beijing: Seismological Press. 2012.

Wu, D.L. Present Crustal Deformation Characteristics in the Northeastern Tibetan Plateau Detected with Time-series InSAR. Lanzhou Institute of Seismology (China). 2021. http://dx.doi.org/10.27491/d.cnki.gzdls.2021.000001.

Xiang, H.F.; Guo, S.M.; Zhang, B.L.; Zhang, W.X.; Yasutaka, I.; He, H.L. Active features of the Eastern Liupanshan piedmont reverse fault zone since late quaternary. J. Seismology and Geology. 1998, (04):34-40. https://kns.cnki.net/kcms2/article/abstract?v=2OF-LjPvQ9e6kNl3gBp3TKMruDAlonjGdqOmwZ1HbtUGV8o8tmbEdUyZST4wNgRfnPNLqpdNucaiNuvuG3SMshd27G9KGjkfxvhdLcBrtFCsnF3Eefe-Ww==&uniplatform=NZKPT&language=CHS.

Xu, H.C.; Wang, H.; Cao, J.L. Slip Rates of the Major faults in the Northeastern Tibetan Plateau and Their Geodynamic Implications. J. Earthquake. 2018, 38(03):13-23. https://kns.cnki.net/kcms/detail/detail.aspx?FileName=DIZN201803002&DbName=CJFQ2018.

Xu, W.J.; Gao M.T. Statistical analysis of the completeness of earthquake catalogs in China mainland. J. Chinese Journal of Geophy. 2014, 57(09):2802-2812. https://doi.org/10.6038/cjg20140907.

Xu, W.J.; Meng, G.J.; Su, X.N. Interseismic Locking Characteristics of the Liupanshan Fault from GPS Observation. J. Earthquake. 2016, 36(03):14-24. https://doi.org/10.3969/j.issn.1000-3274.2016.03.002.

Yang, Z.X.; Waldhuser, F.; Chen, Y.T.; Double-difference relocation of earthquakes in central-western China. J. Journal ofseismology. 2005, 9(2):241-264. https://doi.org/10.1007/s10950-005-3988-z.

Ye, M.S.; Meng, G.J.; Su, X.N. Locking Characteristics and Slip Deficits of the Main Faults in the Northeast Margin of Tibetan Plateau. J. Earthquake. 2018, 38(03):1-12. https://kns.cnki.net/kcms/detail/detail.aspx?FileName=DIZN201803001&DbName=CJFQ2018.

Yuan, D.Y.; Liu, B.C.; Lv, T.Y.; He, W.G.; Liu, X.F.; Gan, W.J. The Study on Seismic Spatial Characters by using the Self-Organized Critical phenomenom. J. Northeastern Seismological Journal. 1998, (04):27-34. https://kns.cnki.net/kcms2/article/abstract?v=2OF-LjPvQ9c0PiCsnwFA4jYVnFp1eiSIzRvhRnUS5yn7umIf8mPXJfcb-d37k2YKnWjzZglLBbBPTGwsYiPwC6otnihN5J-LAIBxqJC9naVDJRJV3JieCw==&uniplatform=NZKPT&language=CHS.

Yuan, D.Y.; Lei, Z.S.; Zhang J.L.; Liu, B.C, Liang, M.J. Textural research of 1219 A. D.Guyuan earthquake in Ningxia HuiAutonomous Region, China, and discussion on its causative structure. J. Acta Seis-mologica Sinica. 2008, 30(6):648-657. https://kns.cnki.net/kcms/detail/detail.aspx?FileName=DZXB200806012&DbName=CJFQ2008.

Zhang, G.M.; Zhang, P.Z. Acodemic Progress on the Mechanism and Forecast for Continental Strong Earthquake in the First Two Years. J. China Basic Science. 2000, (10):4-10. https://kns.cnki.net/kcms2/article/abstract?v=2OF-

LjPvQ9eugIz2LsuNOwZ71BmKowK4m4DEC2eEBO8M0NZ2ruFOAfc6Z27gLFktKoJtHzOkU6QKnZwAtbhaJEek5k3eZRX6HOoRsqWZOfAW410RpMX0fg==&uniplatform=NZKPT&language=CHS.

Zhang, W.Q.; Jiao, D.C.; Zhang, P.Z. Displacement along the Haiyuan fault associated with the great 1920 Haiyuan, China, earthquake. J. Bulletin of the Seismological Society of America. 1987, 77(1):117-131. https://doi.org/10.1785/BSSA0770010117.

Zhang, P.Z.; Burchfiel, B.C.; Molnar, P. Amount and style of late Cenozoic deformation in the Liupanshan area, Ningxia autonomous region, China. J. Tectonics. 1991,10(6):1111-1129. https://doi.org/10.1029/90TC02686.

Zhang, P.Z.; Deng, Q.D.; Zhang, G.M. Strong Earthquake Activity and Active blocks in Chinese Mainland (in Chinese). J. Scientia Sinica (Terrae). 2003, 33(s1):12-20. https://kns.cnki.net/kcms/detail/detail.aspx?FileName=JDXK2003S1001&DbName=CJFQ2003).

Zhang, P.Z,; Wang, Q.; Ma, Z.J. GPS velocity field and active crustal blocks of contemporary tectonic deformation in continental China. J. Earth Science Frontiers. 2002, (02):430-441. https://doi.org/j.issn:1005-2321.2002.02.022.

Zhang, X.; Jiang, Z.S.; Wang, Q.; Wang, X.X.; Cui, D.X.; Zhang, X.L. Invesion for negative dislocation on elastic block boundaries along the northeast margin of Qinghai-Xizang block and prediction for strong earthquake location. J. Acta Seismologica Sinica. 2005, 27(6):620-629. https://doi.org/10.3321/j.issn:0253-3782.2005.06.006.

Zhang, X.L.; Shi, Z.M.; Jiang, F.Y.; Zhu, L.Y.; Wang, X. Research on late tectonic deformation evolvement of Huayuan-Liupanshan Arc Fault and Iits surrounding area. J. Journal of Geodesy and Geodynamics. 2011, 31(03):20-24. https://doi.org/10.14075/j.jgg.2011.03.027.

Zhao, J.; Niu, A.F.; Li, Q.; Yuan, Z.Y. Study on Dynamic Characteristics of Fault Locking and Fault Slip Deficit in the Faults around the Longxi Block. J. Journal of Seismological Research. 2011, 31(03):20-24. https://doi.org/10.14075/j.jgg.2011.03.027.